This article was downloaded by: [National Chiao Tung University 國立交通大學]
On: 28 April 2014, At: 12:07
Publisher: Taylor & Francis
Informa Ltd Registered in England and Wales Registered Number: 1072954
Registered office: Mortimer House, 37-41 Mortimer Street, London W1T 3JH, UK

Journal of Modern Optics
Publication details, including instructions for authors and subscription information:
http://www.tandfonline.com/loi/tmop20

An Active Fibre-optic Interferometric Sensor Based on a Low Finesse Fibre-optic Fabry-Perot

Pie-Yau Chien [a] & Ci-Ling Pan [a]
[a] Institute of Electro-Optical Engineering , National Chiao-Tung University , 1001 Ta Hsueh Road, Hsinchu, Taiwan, 30050, Republic of China
Published online: 01 Mar 2007.

To cite this article: Pie-Yau Chien & Ci-Ling Pan (1991) An Active Fibre-optic Interferometric Sensor Based on a Low Finesse Fibre-optic Fabry-Perot, Journal of Modern Optics, 38:10, 1891-1900, DOI: 10.1080/09500349114552001

To link to this article: http://dx.doi.org/10.1080/09500349114552001

PLEASE SCROLL DOWN FOR ARTICLE

Taylor & Francis makes every effort to ensure the accuracy of all the information (the "Content") contained in the publications on our platform. However, Taylor & Francis, our agents, and our licensors make no representations or warranties whatsoever as to the accuracy, completeness, or suitability for any purpose of the Content. Any opinions and views expressed in this publication are the opinions and views of the authors, and are not the views of or endorsed by Taylor & Francis. The accuracy of the Content should not be relied upon and should be independently verified with primary sources of information. Taylor and Francis shall not be liable for any losses, actions, claims, proceedings, demands, costs, expenses, damages, and other liabilities whatsoever or howsoever caused arising directly or indirectly in connection with, in relation to or arising out of the use of the Content.

This article may be used for research, teaching, and private study purposes. Any substantial or systematic reproduction, redistribution, reselling, loan, sub-licensing, systematic supply, or distribution in any form to anyone is expressly forbidden. Terms & Conditions of access and use can be found at http://www.tandfonline.com/page/terms-and-conditions

JOURNAL OF MODERN OPTICS, 1991, VOL. 38, NO. 10, 1891–1900

An active fibre-optic interferometric sensor based on a low finesse fibre-optic Fabry–Perot

PIE-YAU CHIEN and CI-LING PAN

Institute of Electro-Optical Engineering, National Chiao-Tung University, 1001 Ta Hsueh Road, Hsinchu, Taiwan 30050, Republic of China

(*Received 30 October 1990; revision received 1 February 1991*)

Abstract. We demonstrate a novel active fibre-optic interferometric sensor based on a temperature-stabilized low-finesse fibre-optic Fabry–Perot. In this apparatus, information on the optical phase was extracted from the frequency shift of the He–Ne laser of which the cavity length was thermally tuned to compensate change in the interference signal. It is shown that an improvement in the stability of the interference signal by two orders of magnitudes can be realized. The tracking achievable between the Fabry–Perot interferometer and the laser was better than 1 part in 10^8. That is, the relative frequency stability of the laser was $\leqslant 1{\cdot}0 \times 10^{-8}$ over an interval of tens of minutes. Detection of a change of 5 nm in the optical path length of the fibre-optic Fabry–Perot was also demonstrated. The dynamic range of this interferometer is over 40 dB and the linearity characteristics are excellent. These performance characteristics were limited by the long-term thermal drift of the apparatus, not the low reflectivity of the fibre ends of the Fabry–Perot interferometer.

Downloaded by [National Chiao Tung University] at 12:07 28 April 2014

1. Introduction

Nearly a decade ago, Shajenko and Green [1] first proposed that interferometric hydrophones could be actively stablized by using a tunable laser in a feedback configuration. Since then, these so-called active laser interferometers have been investigated by a number of authors [2–5]. In these interferometers, the change in the interference signal was compensated by tuning the frequency of the laser such that the change in the optical phase was nulled. The theoretical limit of measurement resolution was determined by the linewidth of the laser, while the laser tuning range and the optical path length of the interferometer determined the measurement range. It is interesting to contemplate a fibre-optic version of the active interferometer. In particular, an active fibre-optic interferometric sensor based on a fibre-optic Fabry–Perot interferometer (FFPI) [6–13] is attractive. The FFPI's are very compact and can be easily packaged such that they are immune to environmental disturbances. Basically, there are two types of FFPI's. One is the high-finesse type which uses an optical fibre with ends coated as high reflectivity mirrors or with butt-coupled mirrors at both ends [6–10]. The other is the low-finesse type for which both ends were just cleaved and hence could be fabricated very easily [11–13]. The sensitivity, $\Delta S/\Delta\phi$, of a high-finesse type FFPI is in general superior to that of a two-beam type interferometer because of steeper slope of its transmission function [14]. Here ΔS represents the change in the interference signal and $\Delta\phi$ is the change in the optical phase due to variation in the optical path length of the sensor. Nevertheless, it should be pointed out that the laser phase noise operates through the same discriminator slope as the signal so that the signal to noise ratio remains unchanged in the short

0950–0340/91 $3·00 © 1991 Taylor & Francis Ltd.

noise limit. Furthermore in some applications, the linearity and dynamic range characteristics of the interferometric fibre sensor are more important than its sensitivity. The high-finesse type FFPI is not suited for such applications: except in the region around the resonances, there exist wide ranges of optical path length for which the output signal of the interferometer is very weak. In this paper, we present for the first time, the operation principles and experimental realization of an active fibre-optic interferometric sensor based on a low-finesse FFPI. By employing a deep phase modulation technique, we show experimentally that a low-finesse FFPI is indeed equivalent to conventional two-beam type interferometers. Simultaneous stabilization of the interference signal and the operation wavelegnth of the laser was demonstrated. We have also measured the static change in the optical path length of the order of nanometers. The linearity and dynamic range characteristics of this sensor is examined. We point out that the basic sensitivity limit of the active FFPI sensor is dominated by the long-term thermal drift of the apparatus, not the low reflectivity of the fibre ends.

Downloaded by [National Chiao Tung University] at 12:07 28 April 2014

2. Basic principles

Let us consider a fibre-optic Fabry–Perot interferometer of length L. The intensity of the transmitted light at the output port of the interferometer is given by

$$I = I_0 \frac{(1-R)^2}{(1-R)^2 + 4R\sin^2(\phi/2)}, \tag{1}$$

where I_0 is the peak transmitted intensity corresponding to $\phi = 2p\pi$, p is an integer, R is the Fresnel intensity reflection coefficients of the fibre ends, ϕ is the phase delay for a round trip through the fibre and is given by

$$\begin{aligned}\phi &= 2kL \\ &= 4\pi nLv/c,\end{aligned} \tag{2}$$

where k is the propagation constant and L is the fibre length, v is the laser frequency, c is the velocity of light in vacuum and n is the mean refractive index of the core of the fibre. For as cleaved fibre ends, $R \ll 1$, equation (1) reduces to a sinusoidal function of L;

$$I = \bar{I} + I_m \cos 2kL, \tag{3}$$

where $\bar{I} = I_0 - I_m$ and $I_m = 3RI_0$, which is a factor of R smaller than that of a high-finesse type FFPI. Equation (3) is of the same form as the transmission function of a Mach–Zehnder or Michelson interferometer. This is reasonable, since multiple reflection effects can be ignored for $R \ll 1$. Consequently, a low-finesse type FFPI should exhibit the same linearity and dynamic range characteristics as these two-beam type interferometers.

When the fibre is path-length modulated at the angular frequency ω, the a.c. components of the detected interference signal becomes

$$\begin{aligned}I_{\text{det}} &= I_m \cos(\phi_m \sin\omega t - \phi) \\ &= I_m \left\{ \left[J_0(\phi_m) + 2\sum_{n=1}^{\infty} J_{2n}(\phi_m) \cos 2n\omega t \right] \cos\phi \right. \\ &\quad \left. + \left[2\sum_{n=1}^{\infty} J_{2n-1}(\phi_m) \sin(2n-1)\omega t \right] \sin\phi \right\},\end{aligned} \tag{4}$$

where ϕ_m is the maximum phase deviation due to modulation of the fibre length, $J_n(\phi_m)$ is the Bessel function of order n. The amplitude of the output signal of the synchronous detection circuit used for demodulating I_{det} at the fundamental frequency, ω, is then:

$$V_0 = 2KI_m J_1(\phi_m) \sin \phi, \tag{5}$$

where K is constant representing the system gain of the synchronous detection circuit.

If the amplitude of the sinusoidal waveform employed as the phase modulation signal in equation (4) is adjusted such that ϕ_m is much larger than π radians, the so-called deep phase modulation condition is operative [15]. Under this condition, the sinusoidal waveform can be approximated by the triangular waveform within some effective time periods, T_{eff}. Within these periods, the optical phase is linearly swept such that a beat frequency is generated:

$$I_{det} \propto \cos(\omega_{eff} t - \phi), \tag{6}$$

where $\omega_{eff} = B(2\pi/T_{eff})$, B is an integer. The value of ω_{eff} can in principle be any integral harmonics of the modulation frequency, depending on the modulation amplitude. For this work, $T_{eff} = t_2 - t_1$, where t_1 and t_2 are respectively the 20% and 70% points in the half period of the phase modulation signal. Experimental observation of ω_{eff} would be an independent confirmation of equation (3). That is, the output format of a low-finesse FFPI is identical to that of a two-beam interferometer.

Let us consider the sensor in the configuration of an active interferometer. We further assume the mean index of refraction of the fibre core, n, is a constant. From equation (2), we can show that

$$\Delta\phi = \frac{4\pi n}{c}(v\Delta L + L\Delta v). \tag{7}$$

In an active interferometer, the phase change is nulled by tuning the frequency of the laser such that

$$\Delta v = -\left(\frac{v}{L}\right)\Delta L. \tag{8}$$

External disturbances as well as actual change in the length of the fibre contribute to ΔL. The scale factor, v/L, is a characteristic quantity of the active FFPI. Equation (8) indicates that the range of ΔL that can be measured for a given tuning range of the laser, Δv, is linearly proportional to L. By employing a laser with sufficiently large tuning range or appropriate choice of L, either $\Delta L \ll \lambda$ or $\Delta L \gg \lambda$ can be measured.

3. Experimental methods

The block diagram of our experimental set-up is shown in figure 1. An internal-mirror He–Ne laser (Spectra Physics model 155, $\lambda = 0{\cdot}633\ \mu m$), oscillating in two axial modes, was used as the light source. A polarizer with an extinction ratio of 30 db was used to select the one of two orthogonal modes of the He–Ne laser. The relative output power level of the two modes depends on the operating point, i.e., the cavity length of the laser. An isolator was used to prevent the optical feedback from fibre

Downloaded by [National Chiao Tung University] at 12:07 28 April 2014

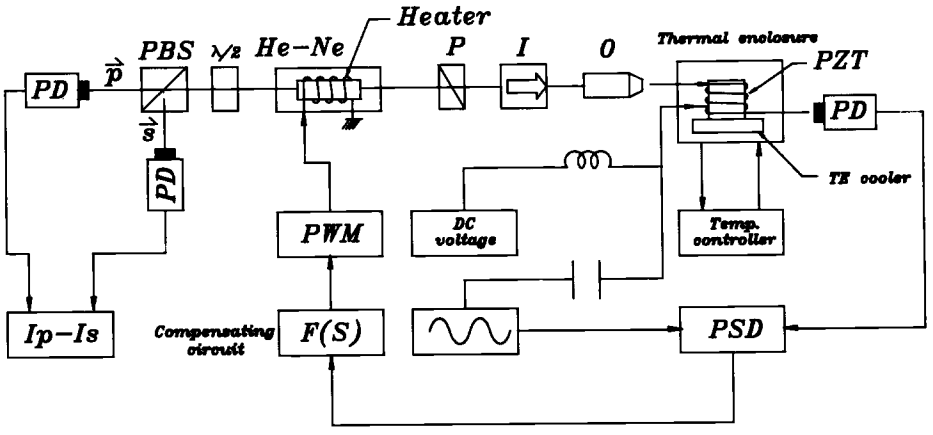

Figure 1. The block diagram of the experimental set-up; P, polarizer; I, isolator; O, objective lens; PD, photodetector; PZT, piezoelectric transducer; PSD, phase sensitive detector; PWM, pulse width modulator; PBS, polarization beam splitter; F(S), the Laplace transfer function of the compensating circuit.

ends. A 10× objective lens focused the laser light into the fibre core. The Fabry–Perot interferometer consisted of a 30 cm length of single-mode non-polarization-maintaining fibre with as cleaved ends. The fibre was wound several times around a disk-type piezoelectric transducer (PZT) used for path-length modulation in the interferometer. For passive temperature stabilization, the FFPI was mounted on top of a thermoelectric cooler (TE) and enclosed in a 4 cm × 4 cm × 2 cm acrylic box. The demodulation circuit for the detection of the temperature variation of the FFPI was of the bridge-type with balanced resistors and a precision thermistor as the temperature sensor. With a stable modulation signal, temperature variations as small as 2×10^{-4} C can be detected by standard phase sensitive detection (PSD) techniques. Recently we have shown that internal-mirror He–Ne lasers can be frequency-stabilized by using the so-called thermal phase lock loop [16]. The same principle was applied here and a block diagram of the control circuit is shown in figure 2. An offset between the room temperature and the controlled temperature in the box was necessary to increase the system bandwidth of the servo loop. In this experiment, the operating temperature in the box was necessary to increase the system bandwidth of the servo loop. In this experiment, the operating temperature in the enclosed box was selected to be 10°C while the environmental temperature was 20°C. Proportional and integrating (P + I) compensation circuits were also used in the feedback loop to improve the system stability. By proper adjustment of the loop gain and the compensating zero in the PI circuit, a temperature stability of 5×10^{-4}°C with a measurement bandwidth of 1 Hz was achieved. Typical data are shown in figure 3. This level of temperature stability has also been reported by several other groups [17]–[20].

For stabilization of the interference signal, we adjusted the modulation index such that the value of $J_1(\phi_m)$ equals its maximum value for the highest sensitivity. The output signal was amplified and processed by a PSD circuit for demodulating the signal of interest, $2KI_mJ_1(\phi_m)\sin\phi$. This error signal was then used to control the laser frequency until the change in ϕ was nulled.

Downloaded by [National Chiao Tung University] at 12:07 28 April 2014

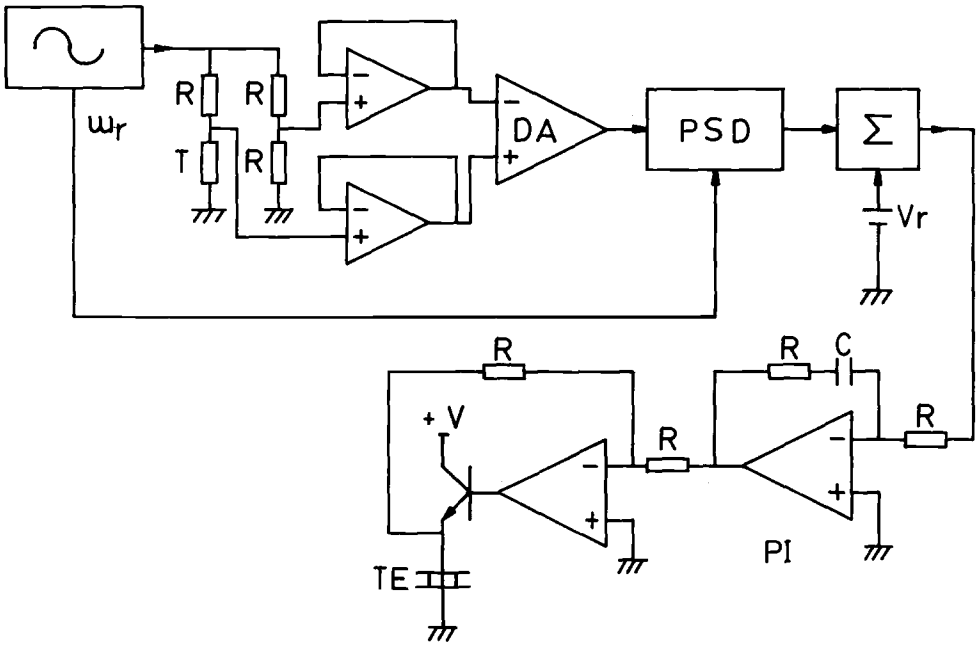

Figure 2. A schematic diagram of the circuit for the temperature controller. ω_r: modulation signal, DA: differential amplifier, PSD: phase sensitive detector, V_r: reference voltage, TE: thermoelectric cooler.

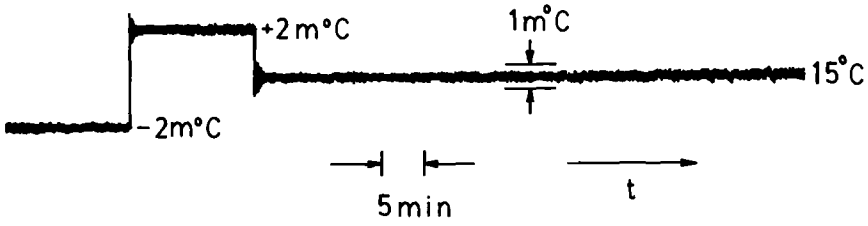

Figure 3. Typical data of the residue temperature fluctuations of the thermally-stabilized FFPI over a period of tens of minutes. $1\,\mathrm{m\,C} = 10^{-3}\mathrm{C}$.

Tuning of the laser frequency was implemented by thermally tuning the laser cavity length. A heater wound around the laser cavity was the control element. A compensating network which consists of an integrator, a zero and a lead-lag circuit [21, 22] was adopted for improving the stability of our servo system. A pulse width modulation (PWM) type power amplifier was used to drive the heater. The heater can only raise the temperature of the laser tube. In order to improve the system response, a pre-heating cycle was required to ensure that the laser tube will always be able to cool down by loosing heat to its surroundings. This was implemented by adjusting the temperature of laser tube until the time constants of the servo system for heating and cooling the laser tube were about equal.

Downloaded by [National Chiao Tung University] at 12:07 28 April 2014

Downloaded by [National Chiao Tung University] at 12:07 28 April 2014

4. Results and discussions

For $\phi_m \gg \pi$, i.e., the optical phase of the FFPI was deeply modulated, the outputs of the photodiode (upper trace) and the modulation signals applied to the PZT (lower trace) for two different modulation amplitudes are shown in figures 4 (*a*) and (*b*) respectively. The waveform in the linearly phase-modulated regions can be examined by time-gating and bandpass filtering techniques [15]. The gated interference signals were indeed found to be sinusoidal. This is in agreement with the predictions of equation 3 to equation (5) and illustrates that the low-finesse FFPI can indeed be treated as a two-beam type interferometer. As a result, signal processing techniques developed for the latter can be employed for the low-finesse FFPI. We note that the frequency of the interference signal as shown in figure 4 is higher than that of the modulation frequency. This is possible by proper adjustments of the magnitudes of ϕ_m and ϕ. In fact, it is possible to obtain a frequency spectrum of I_{det} which contains many higher-order harmonics of ω and with about the same amplitudes. This forms the basis for a novel wide-band optical signal generator and details will be presented elsewhere [23].

We shall next discuss our results on signal stabilization of the FFPI. Figure 5 shows the PSD output under free-running and closed loop conditions (upper trace) as well as a trace of $\Delta I = I_p - I_s$, the difference in intensities of the two orthogonally polarized axial mode, under the closed loop condition (lower trace). The recorder trace of ΔI for the free-running case was similar to that of the PSD output and is not shown for lack of space. The output of the PSD circuit was just the error signal of the servo loop, for which the phase drift due to the change of the fibre length in the FFPI was not included. Thus a trace of excellent signal-to-noise ratio could be obtained as shown in the upper trace of figure 5. The frequency shift of the laser, as represented by change in ΔI, provided a more sensitive discriminator for evaluating the stability of the interference signal. When the servo loop was closed, we observed that the peak-to-peak frequency fluctuation of the laser was less than 5 MHz over a period of tens of minutes (see figure 5, lower trace). This is calibrated using the peak-to-bottom value of ΔI, which corresponds to a shift in the frequency of the laser by one axial mode spacing, ≈ 550 MHz for our laser. Figure 5 thus illustrates that the stability of the interference signal was improved by more than a factor of 110 or two

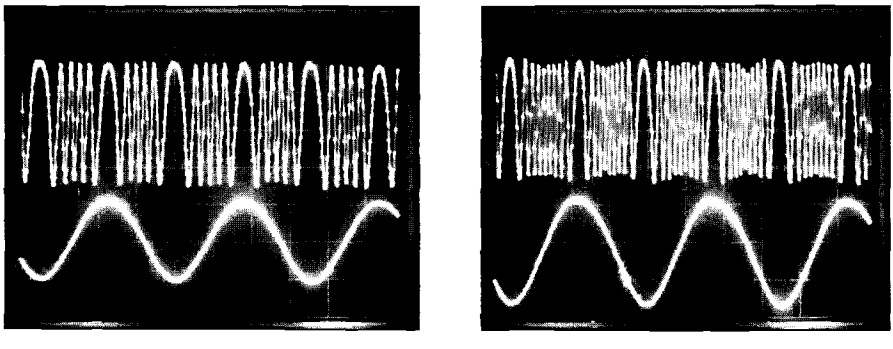

(*a*) (*b*)

Figure 4. Oscilloscope traces of the outputs of photodiode for different phase modulation indices under the deep phase modulation condition. The upper trace is the output of the photodetector; the lower trace is the applied modulation signal to the PZT. (*a*) The applied signal is 2 V peak to peak at 100 kHz. (*b*) The applied signal is 4 V peak to peak at 100 kHz.

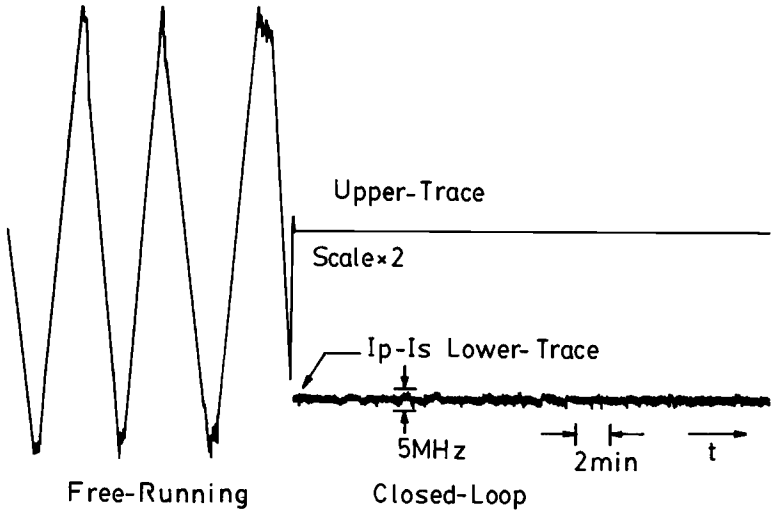

Figure 5. The output of the PSD in figure 1 for the system in free-running and closed loop conditions (upper trace). The corresponding trace for $\Delta I = I_p - I_s$ under closed loop conditions is shown in the lower trace.

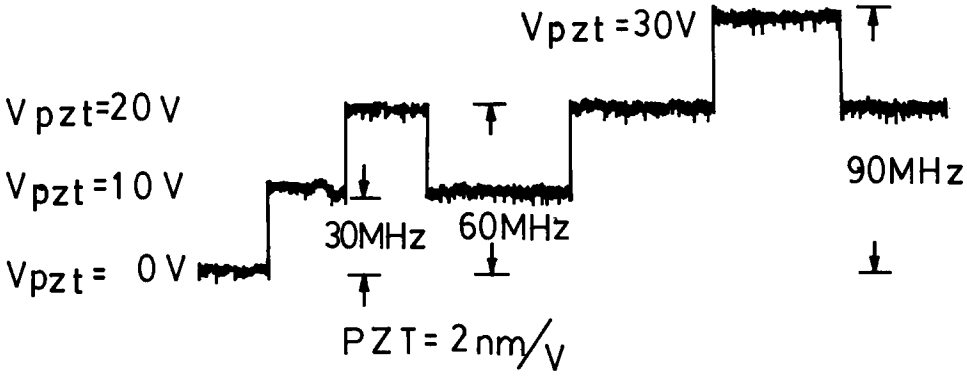

Figure 6. Frequency detuning of the He–Ne laser for different d.c. voltage steps applied to PZT.

orders of magnitudes. Since the residue fluctuation of ΔI is a measure of the fluctuation of the output frequency of the laser, this indicates that the laser was also stabilized at the same time with a relative frequency stability, $\Delta\nu/\nu \leqslant 1 \times 10^{-8}$. In other words, the tracking achievable between the FFPI and the laser was stable to 1 part in 10^8.

Examining equation (5), we see that the amplitude of the demodulated signal of a low-finesse type FFPI is lower than that of a high-finesse type FFPI because of the lower reflectivity ($R \cong 0{\cdot}035$ for $n = 1{\cdot}46$). Previous workers [24–26] have shown that a minimum detectable phase shift $\phi_{\min} \cong 1{\cdot}0 \times 10^{-6}\,\text{rad}\,(\text{Hz})^{-1/2}$ could be achieved by employing PSD techniques. It follows that $\phi_{\min}$ for a low-finesse type FFPI should be $2{\cdot}8 \times 10^{-5}\,\text{rad}\,(\text{Hz})^{-1/2}$. In terms of the frequency shift of the laser source, this corresponds to $\Delta\nu_{\min} \cong 5\,\text{kHz}$ for $L = 30\,\text{cm}$ and a detection bandwidth of 10 Hz.

Downloaded by [National Chiao Tung University] at 12:07 28 April 2014

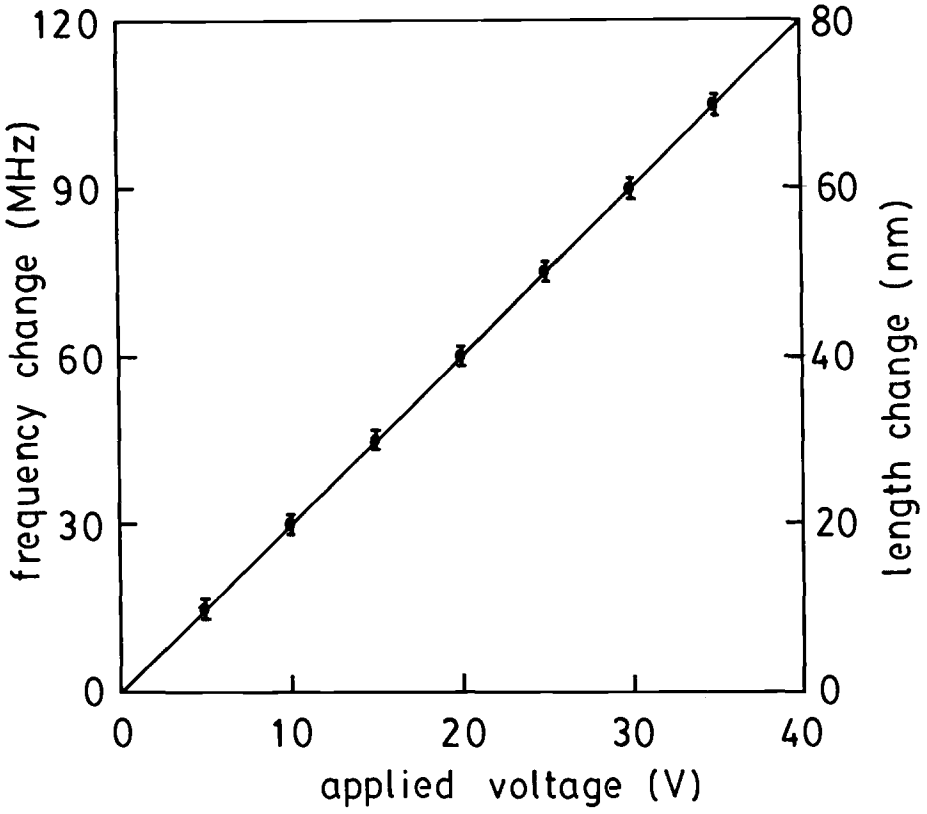

Figure 7. Linearity of optical path length measurement using the active FFPI. The slope of the solid line is 3·2 MHz V^{-1} or 2 nm V^{-1}. The bar indicates residue error of 5 MHz or $\cong$3 nm.

Actually this is limited by the thermal stability of the FFPI. Assuming a thermal expansion coefficient of $1{\cdot}0\times10^{-5}\,C^{-1}$ for typical optical fibres and a residue temperature fluctuation of $5{\cdot}0\times10^{-4}$ C as achieved in this work, $\Delta\nu_{min}=2{\cdot}4$ MHz. This is consistent with our experimental results. Conventional high-finesse Fabry–Perot and two-beam type interferometers also face the same thermal drift problem. Clearly, there is no fundamental advantage in employing a high-finesse type FFPI in the applications discussed above.

Figure 6 illustrates the change in ΔI corresponding to different d.c. voltage steps applied to the PZT with a specification of 2 nm V^{-1}. With $\Delta\phi_{min}=2{\cdot}8\times10^{-4}$ rad $(Hz)^{-1/2}$, equation (7) predicts that $\Delta L_{min}\cong1{\cdot}0\times10^{-3}$ nm $(Hz)^{-1/2}$ if $\Delta\nu\cong0$. As in the previous case, however, thermal drift limits the minimum detectable change in the optical path length. As given in equation (8), $\Delta L_{min}=L(\Delta\nu_{min}/\nu)=3$ nm. This is in good agreement with our experimental results, where a 5 nm change in the path length or a voltage step of 2·5 V could be detected easily. We note that with $\Delta\nu_{min}$ remaining unchanged, ΔL_{min} can be readily improved by an order of magnitude, i.e., in the subnanometer range, by simply reducing L from 30 to 3 cm. Figure 7 demonstrates the linearity of this active sensor. Clearly the data points fall on a solid line with a slope of 3·2 MHz V^{-1} or 2 nm V^{-1}, which corresponds to

Downloaded by [National Chiao Tung University] at 12:07 28 April 2014

the scale factor, 1·6 MHz nm^{-1}, that we discussed in equation (8). Since the tuning range of our laser is approximately 1 GHz, the measurement range would be 0·6 μm. This corresponds to a dynamic range of 40 dB. By employing a light source with broader tuning range, e.g., a laser diode, this can be further increased.

5. Conclusions

The basic concepts and experimental realization of a novel fibre optic interferometric sensor based on a low-finesse fibre-optic Fabry–Perot interferometer (FFPI) have been presented. To begin with, we demonstrate experimentally, for the first time, that the output format of a low-finesse FFPI is indeed identical to that of a Michelson or Mach–Zehnder interferometer. By employing the low-finesse FFPI in the configuration of an active interferometer, we were able to improve the stability of the interference signal by two orders of magnitude. The frequency of the laser was also stabilized at the same time, with a relative frequency stability of $\Delta\nu/\nu \cong 1{\cdot}0 \times 10^{-8}$ over a period of tens of minutes. Detection of a change of 5 nm in the optical path length of the FFPI was also demonstrated. These performance characteristics were limited by the long-term thermal drift of the apparatus, not the low reflectivity of the fibre ends of the FFPI. If a measurement resolution in the range of subnanometer is desired, this can be achieved with a shorter length of fibre. The measurement range, however, would be reduced by the same factor. The dynamic range of the present active sensor was more than 40 dB. Excellent linearity characteristics was also observed.

Acknowledgments

This work was partially supported by the National Science Council of the Republic of China. We would like to thank the referees for valuable comments.

References

[1] Shajenko, P., and Green, E. L., 1980, *Appl. Optics*, **19,** 1895.
[2] Olsson, A., Tang, C. L., and Green, E. L., 1980, *Appl. Optics*, **19,** 1897.
[3] Shi, Y. C., and Olsson, N. A., 1985, *Appl. Optics*, **24,** 2287.
[4] Yoshino, T., Nara, M., Mnatzakanian, S., Lee, B. S., and Strand, T. C., 1987, *Appl. Optics*, **26,** 892.
[5] Lin, Yi-Jyh, and Pan, Ci-Ling, 1991, *Appl. Optics*, **30,** 1648.
[6] Stone, J., 1985, *Electron. Lett.*, **21,** 504.
[7] Franzen, D. C., and Kim, E. M., 1981, *Appl. Optics*, **20,** 3391.
[8] Kist, R., and Sohler, W., 1983, *J. Lightwave Technol.*, **LT-1,** 105.
[9] Stone, J., and Marcuse, D., 1986, *J. Lightwave Technol.*, **LT-4,** 382.
[10] Yoshino, T., Kurosawa, K., Itoh, K., and Ose, T., 1982, *IEEE J. quant. Electron.*, **QE-18,** 1624.
[11] Ito, T., 1986, *Appl. Optics*, **25,** 1072.
[12] Kersey, A. D., Jackson, D. A., and Corke, M., 1983, *Optics. Commun.*, **45,** 71.
[13] Seki, Y., and Noda, K. I., 1987, *J. Lightwave Technol.*, **LT-5,** 961.
[14] Petuchowski, S. J., Giallorenzi, T. G., and Sheem, S. K., 1981, *IEEE J. quant. Electron.*, **QE-17,** 2168.
[15] Chien, Pie-Yau, and Pan, Ci-Ling, 1991, *IEEE Photon. Technol. Lett.*, **3,** 284.
[16] Chien, Pie-Yau, and Pan, Ci-Ling, 1991, *Rev. scient. Instrum.*, **62,** 933.
[17] Sarid, D., and Cannell, D. S., 1974, *Rev. scient. Instrum.*, **45,** 1082.
[18] Dratler, J. Jr, 1974, *Rev. scient. Instrum.*, **45,** 1435.

Downloaded by [National Chiao Tung University] at 12:07 28 April 2014

[19] FEATHERSTONE, J. D. B., and DICKINSON, N. A., 1977, *J. Phys.* E, **10,** 334.
[20] HANDSCHY, M. A., 1980, *J. Phys.* E, **13,** 998.
[21] PAN, CI-LING, JEAN, P.-Y., KUO, C.-C., HSIEH, T.-C., and LEI, T. T., 1985, *Appl. Optics*, **24,** 3430.
[22] PAN, CI-LING, and JEAN, P.-Y., 1986, *Appl. Optics*, **25,** 2126.
[23] CHIEN, PIE-YAU, and PAN, CI-LING, 1991, *Rev. scient. Instrum.* (to be published).
[24] EICHEN, E., and SILLETTI, A., 1987, *J. Lightwave Technol.*, **LT-5,** 1377.
[25] JACKSON, D. A., DANDRIDGE, A., and SHEEM, S. K., 1980, *Optics Lett.*, **5,** 139.
[26] JACKSON, D. A., PRIEST, R., DANDRIDGE, A., and TVETEN, A. B., 1980, *Appl. Optics*, **19,** 2926.

Downloaded by [National Chiao Tung University] at 12:07 28 April 2014